LA-UR- 08-5281

Approved for public release; distribution is unlimited.

Title:	Air Shower Detectors in Gamma-Ray Astronomy
Author(s):	Gus Sinnis
Intended for:	New Journal of Physics

Form 836 (7/06)

Air Shower Detectors in Gamma-Ray Astronomy

G Sinnis

Physics Division, Los Alamos National Laboratory, Los Alamos, NM 87545

E-mail: gus@lanl.gov

Abstract. Extensive air shower arrays directly detect the particles in an extensive air shower that reach the observation altitude. This detection technique effectively makes air shower arrays synoptic telescopes - they are capable of simultaneously and continuously viewing the entire overhead sky. Typical air shower detectors have an effective field-of-view of 2 sr and operate nearly 100% of the time. These two characteristics make them ideal instruments for studying the highest energy gamma rays, extended sources, and transient phenomena. Until recently air shower arrays have had insufficient sensitivity to detect gamma-ray sources. Over the past decade, the situation has changed markedly. Milagro, in the U.S, and the Tibet ASγ array in Tibet, have detected very-high-energy gamma-ray emission from the Crab Nebula and the active galaxy Markarian 421 (both previously known sources). Milagro has discovered TeV diffuse emission from the Milky Way, three unidentified sources of TeV gamma rays, and several candidate sources of TeV gamma rays. Given these successes and the suite of existing and planned instruments in the GeV and TeV regime (AGILE, GLAST, H.E.S.S., VERITAS, CTA, AGIS, and IceCube) there are strong reasons for pursuing a next generation of EAS detectors. In conjunction with these other instruments the next generation of EAS instruments could answer long-standing problems in astrophysics.

1. Introduction

There are two general types of detectors used in very-high-energy (VHE) gamma-ray astronomy, imaging atmospheric Cherenkov telescopes (IACTs), or arrays of such instrument, and extensive air shower (EAS) arrays. (For this paper I define VHE gamma rays as the >100 GeV energy band.) The two techniques are complementary - while IACTs have far superior instantaneous sensitivity, angular, and energy resolution, EAS arrays have a large field-of-view and operate continuously. Together these two types of instruments are sensitive to an enormous range of physical phenomena from the most violent and extreme objects in the universe.

The first generation of extensive air shower arrays to be used for gamma-ray astronomy were typically composed of small plastic scintillators ($\sim$1 m^2 each) distributed over large areas (40,000 - 230,000 m^2). With an active area comprising $< 1\%$ of the enclosed area these arrays had high energy thresholds ($\sim$100 TeV), which limited their sensitivity. The CYGNUS [1] and CASA [2] arrays where the largest of these type of instruments. The energy threshold of the CASA array was $\sim$200 TeV, making extragalactic astronomy impossible and Galactic astronomy difficult. No unequivocal evidence for sources of gamma rays was found with these instruments. The path forward from this generation of instruments was clear - lower the energy threshold. Two different approaches have been successfully employed to accomplish this goal. The Milagro detector[3] in Los Alamos, NM uses the water Cherenkov technique to provide an active detector area that is essentially equal to the physical area enclosed by the detector. This dense sampling of the air shower yields a median energy of 2 TeV to gamma rays from a Crab-like source. The Tibet ASγ detector [4] in Tibet has obtained a similar energy response by locating their telescope at an extreme altitude - 4300 m above sea level. Next to the ASγ detector, ARGO has begun operations and detected the Crab Nebula [5]. ARGO combines the high altitude of ASγ and the dense sampling of Milagro, through the use of resistive plate chambers (RPCs). The low energy-threshold of these instruments has enabled high significance detections of the Crab Nebula and the extragalactic source Mrk 421, an active galaxy at a redshift of 0.03. These detections, were essential in establishing the sensitivity of the technique. More recently, Milagro has detected the Galactic diffuse emission at energies above 10 TeV and three new sources of TeV gamma rays. Measurement of the Galactic diffuse emission provides critical information on the cosmic-ray (both protons and electrons) intensity and spectrum throughout our Galaxy at energies near 100 TeV.

The strength of EAS arrays (relative to IACTs) lies in their ability to continuously view a large fraction of the sky. This capability makes them well suited to study extended sources, such as the Galactic diffuse emission, measure the spectra of Galactic sources at the highest energies (near or beyond 100 TeV), and study the transient universe. The current suite of instruments have indicated the potential of the technique, however large gains in sensitivity are possible and a next generation of EAS detector will have an enormous discovery potential. In this paper I will briefly explain the detection technique,

review the recent acheivements of the current generation of synoptic telescopes and discuss a the future development of synoptic VHE telescopes. For information on previous generations of EAS arrays see for example [6, 7].

2. Extensive Air Showers and Their Detection

When a high-energy gamma ray enters the earth's atmosphere its interactions are predominantly electromagnetic. The first interaction is typically the creation of an electron-positron pair. These particles then undergo bremsstrahlung interactions, generating additional high energy gamma rays. This process continues until the average energy per electromagnetic particle drops to the critical energy, ~84 MeV. At this point the number of particles in the air shower is at a maximum and the altitude at which this occurs is referred to as "shower maximum". As the air shower continues to propagate through the atmosphere the energy loss is dominated by ionization, not by the creation of additional particles, and the number of particles in the air shower decreases with increasing atmospheric depth. The number of electromagnetic particles as a function of atmospheric depth (the longitudinal development of the air shower) is well described (on average) by Approximation B [11], see Figure 1. The fluctuations in the development of the EAS are dominated by the fluctuations in the depth of the first interaction. The distribution of first interaction depths can be parameterized as

$$p(t_1) = (1/t_{int})exp(-t_1/t_{int}),$$

where t_1 is the depth of the first interaction and t_{int} is the mean interaction length (where t_1 and t_{int} are expressed in units of the radiation length) [12]. Figure 2 shows the correlation between the number of electromagnetic particles reaching the ground and the depth of the first interaction. It can be seen from the figure that while the average number of electromagnetic particles that reach the ground is ~75 (for a 100 GeV primary), the resulting distribution will be rather broad, with a full-width at half maximum spanning the range ~50-175 particles. As we will see below, it is these fluctuations in the development of the air shower that limit the energy resolution of an EAS array.

Using the information above one can make a rough estimate of the response of an EAS array without invoking detailed Monte Carlo simulations of a specific detector design. The sensitivity of an array is determined by the effective area of the array as a function of energy, the ability to reject the cosmic-ray background, the angular resolution, and the energy resolution of the array. The relative importance of each of these parameters depends upon the type of gamma-ray source under study.

The energy response of the detector can be studied by imposing a simple trigger condition and studying the efficiency of satisfying this trigger condition as a function of primary gamma-ray energy and the altitude of the detector. In Figure 3 we have imposed a trigger requirement of 100 electromagnetic particles each with at least 10 MeV at observation level. Since gamma rays out number electrons and positrons by a

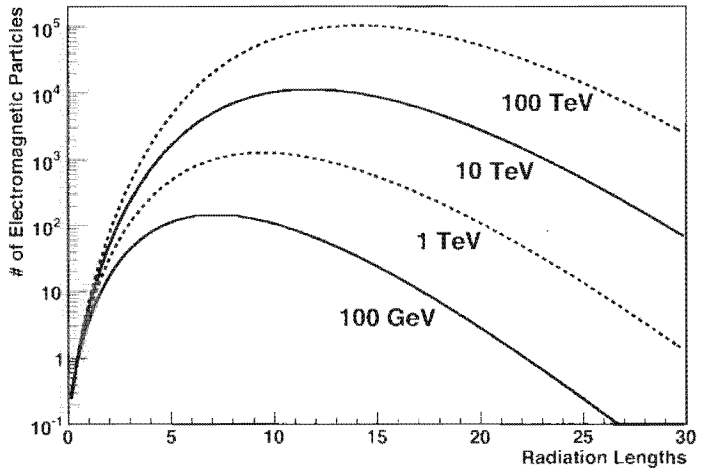

Figure 1. The longitudinal development of an extensive air shower as given by approximation B for several different primary gamma-ray energies. The x-axis is the atmospheric depth expressed as the number of radiation lengths. The y-axis gives the number of electromagnetic particles in the air shower. Sea level is ~28 radiation lengths of atmosphere, 2600 m above sea level is ~20 radiation lengths, 4300 m above sea level is ~16.5 radiation lengths, and 5200 m above sea level is ~14.7 radiation lengths.

factor of ~6, the ability to detect the gamma rays in an EAS is critical to achieving a low energy threshold. The density of sensitive detector elements determines the fraction of particles falling within the enclosed area that are detected, thus a dense array will typically have a lower energy threshold than a sparse one (if they are equally sensitive to the different components of the EAS). Figure 3 shows that, in principle, an EAS array with significant sensitivity at 100 GeV can be built. However to achieve this level of sensitivity the array must be constructed at an extreme altitude (>4000 m above sea level), be sensitive to the gamma-ray component of the EAS, and densely sample the air shower.

Once the array has triggered on an EAS it is necessary to reconstruct the properties of the primary particle: its energy, its direction, and its nature (gamma ray or hadronic particle). We will discuss each of these in turn.

Energy Resolution In Figure 4 we show the average energy reaching the observation altitude as a function of primary gamma-ray energy, where the average has been taken over those events that satisfy the trigger condition described above. At an energy where the trigger efficiency is one, roughly 10% of the primary gamma-ray energy (in the form of electromagnetic particles) reaches an altitude of 5200 m above sea level. Note that once the trigger efficiency (as defined from Figure 3) falls below unity, the energy reaching the ground is independent of the primary gamma-ray energy (it is determined by the trigger condition). Thus, an EAS array can not measure the energy of these

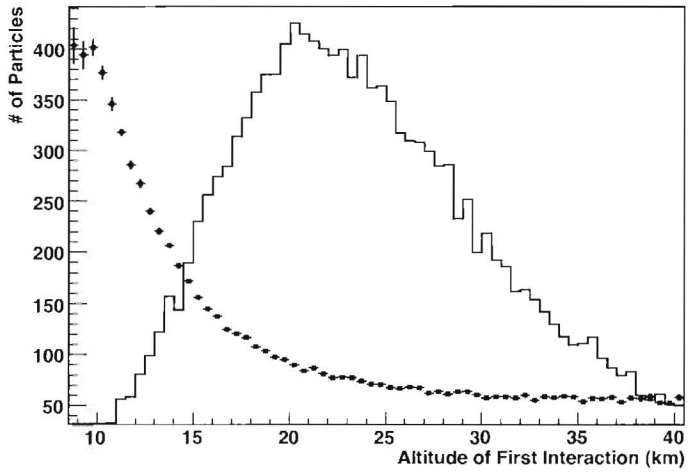

Figure 2. The number of electromagnetic particles with energy above 10 MeV as a function of the depth of the first interaction (shown as the squares with error bars). The histogram shows the distribution of first interaction altitudes (in which case the y-axis is in arbitrary units). The primary gamma ray had an energy of 100 GeV and the observation altitude was taken to be 5200 m above sea level. This figure was generated using the CORSIKA simulation package [13].

events, but can only place an upper bound on the energy of the primary gamma ray.

In practice an EAS array can accurately measure the energy that reaches the ground and the energy resolution of an EAS array is almost completely determined by the fluctuations in the development of the air shower (see Figure 2), in particular the height of shower maximum. The magnitude of the fluctuations is dependent upon the primary energy and the observation altitude. Figure 5 shows the expected energy resolution, accounting for both the shower fluctuations and the measurement errors, for two different observation altitudes.

Angular Resolution The pointing accuracy of an EAS array is ultimately limited by the momentum distribution of the electromagnetic particles that reach the ground. To estimate the best posible angular resolution one can sum the momentum components of the particles in the ground plane and in the z-direction (perpendicular to the ground plane). Figure 6 shows the direction (from zenith) of the net momenta of all electromagnetic particles with energy above 10 MeV as a function of primary energy. The events were generated from zenith, thus this angle from zenith represents the best achievable angular resolution for an EAS array located at the observation altitude of 5200 m above sea level. This figure demonstrates that at "low" energies (<300 GeV) the angular resolution of an EAS detector can not be better than 0.4-0.5 degrees. At higher energies, the angular resolution improves but will be limited by the finite sampling of the shower particles and the corrections to the measured arrival times that are required to reconstruct an EAS. The actual angular resolution is determined by the number of

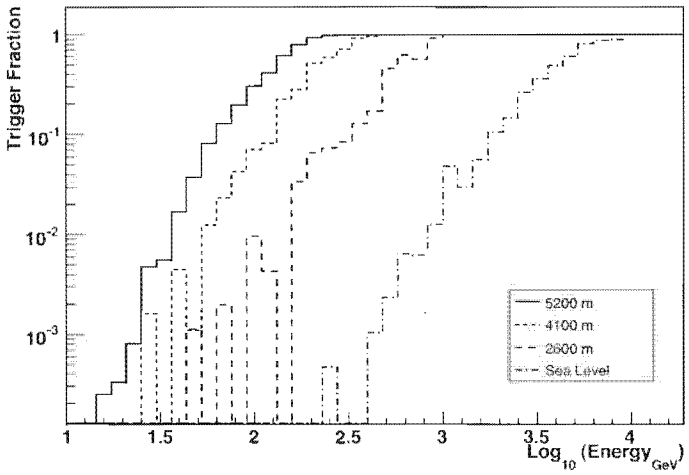

Figure 3. The fraction of gamma-ray primaries that result in an EAS with more than 100 particles each of more than 10 MeV energy as a function of primary energy. The results for four different observation levels are shown. To simplify the interpretation of the figure all events were generated from zenith. This figure was generated using the CORSIKA simulation package [13].

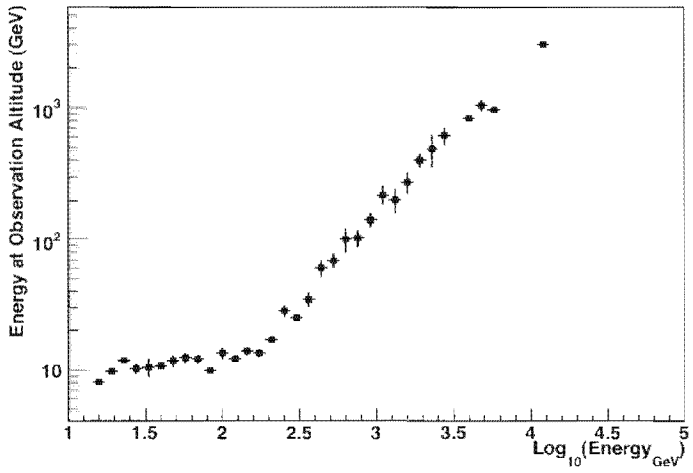

Figure 4. The energy reaching the ground as a function of primary gamma-ray energy for an observation altitude of 5200m above sea level. The figure shows the average energy reaching the ground for events that satisfy the trigger condition defined in the text. (These events were generated from zenith.) This figure was generated using the CORSIKA simulation package [13].

particles detected, the radial extent of the detected particles, the timing resolution of the measurements, and the ability to correct for the non-planar aspects of the EAS

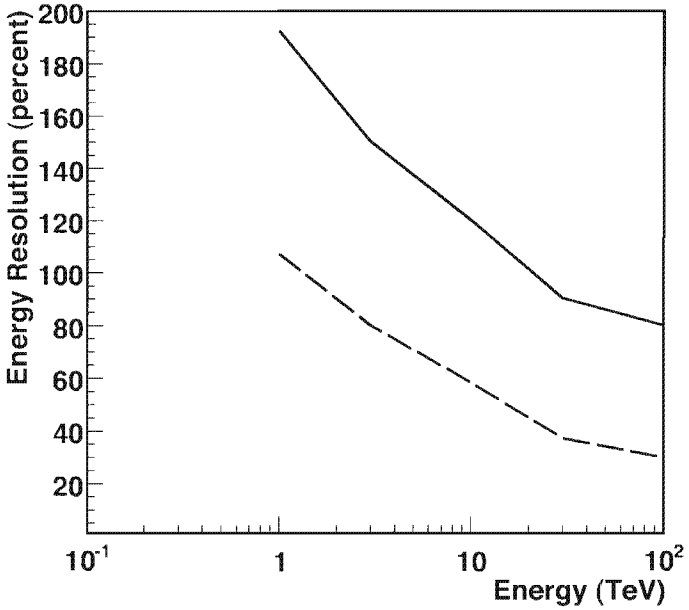

Figure 5. The energy resolution as a function of primary gamma-ray energy. The solid line corresponds to an observation altitude of 2630 m above sea level and the dashed line to an observation altitude of 4100 m above sea level. Figure courtesy of Andrew Smith.

shower front. (The shower front is a cone centered on the shower core.) The magnitude of this last correction is demonstrated in Figure 7, which shows the angular resolution of an idealized detector before and after the affect of a correction for the curvature of the shower front is made. A correction is made for both the distance from the shower core and the number of detected particles at each location. (This correction accounts for the statistical affect of making multiple measurements of a distribution of particle arrival times and recording only the first arrival time measured.) At the highest energies, $>$ 10TeV, an angular resolution of $\sim$0.2 degrees could be acheivable.

Background Rejection Background rejection in an EAS array is accomplished by the detection and identification of the penetrating component of extensive air showers initiated by hadronic cosmic rays. (While other methods have been proposed, they have yet to be demonstrated in an astronomical observation [14].) The efficacy of the background rejection is ultimately limited by the number of muons and hadrons that survive to the observation altitude. The surviving particle must have sufficient energy to be differentiated from the electromagnetic portion of the cascade. Below, we assume an observation altitude of 5200 m and a muon energy threshold of 500 MeV. Figure 8 shows the average number of muons and hadrons that reach the ground as

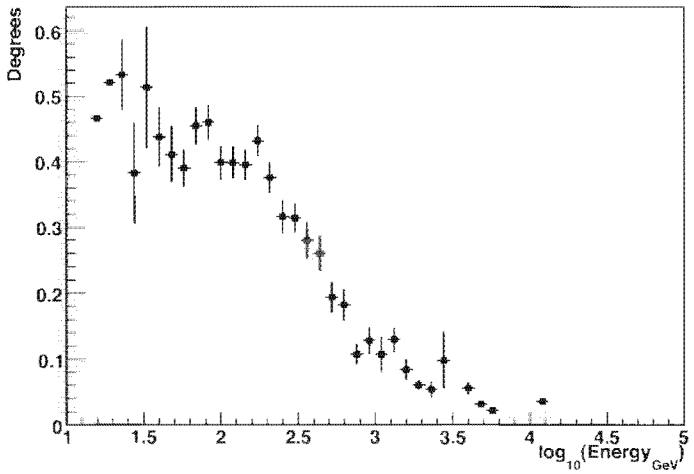

Figure 6. The average direction of the net momenta of all electromagnetic particles with energy greater than 10 MeV as a function of primary energy. An observation altitude of 5200 m above sea level was assumed and all events were generated from zenith. Thus, the y-axis represents the best possible angular resolution attainable for an EAS array at this elevation.

a function of primary proton energy. While the muon content of an EAS changes slowly with decreasing altitude, the hadronic component of an EAS decreases with increasing atmospheric depth. (For an observation altitude of 2600 m the number of surviving hadrons is $\sim 1/3$ the number at 5200 m, while the number of surviving muons is essentially unchanged.) Figure 8 shows that on average a primary proton with energy of 300 GeV will yield 10 energetic muons at ground level. Since the Poisson probability of observing zero when one expects 10 is about 4×10^{-5} one would expect to have excellent rejection capabilities even at these relatively low energies. However, there are two effects that tend to decrease the background rejection capabilities of an EAS array at low energies. First, the fluctuations in the number of surviving muons are larger than Poisson. For example, for a 2 TeV proton primary the Gaussian width of the muon number distribution is about $2.5\sqrt{(N_\mu)}$. Thus, there are are more events with zero muons than a straightforward Poisson calculation would conclude.

The second affect is that the fluctuations in the shower size (the number of electromagnetic particles at observation level) are quite large. Since the shower size is the observable parameter (not the primary energy), one must examine the muon number as a function of the shower size. This is shown in Figure 9, where we have plotted the detected muon number versus the detected shower size for the proposed future detector, Tibet+MD (see the "Future Directions" section for further details on the Tibet+MD detector). A minimum muon energy of 1.2 GeV was requried. The results are shown for both cosmic-ray and gamma ray induced air showers. At a detected shower size of $\sim$1300, with a corresponding gamma-ray energy of $\sim$100 TeV, this detector would

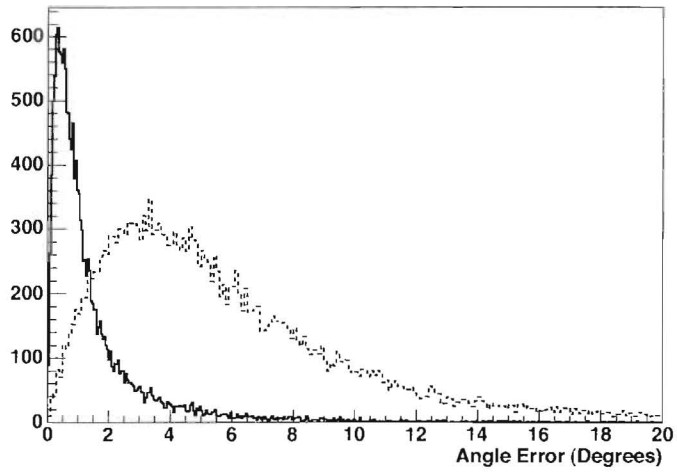

Figure 7. The point spread function for the reconstruction of the direction of the primary particle. The angular reconstruction is performed using the actual particle arrival times, positions, and energies. The solid line shows the point spread function after an energy dependent curvature correction is made to the particle arrival times and the dashed line shows the point-spread function before these corrections are made. Gamma rays generated on an $E^{2.6}$ differential spectrum, with energies between 100 GeV and 100 TeV, and satisfying the trigger condition described above were used in this figure.

be essentially background free, rejecting 99.99% of the cosmic-ray background. Once an EAS array (or any instrument) is in a background free environment, its sensitivity is the inverse of the effective area of the instrument multiplied by the amount of time spent viewing a source. Thus, with a comparable effective area to an IACT array, an EAS array, with more than an order of magnitude greater time on source, will have substantially better sensitivity to the highest energy gamma rays, even to a known source.

At lower energies, while not background free, a substantial fraction of the background can be rejected with the EAS technique, if the detector has a sufficiently large muon detector. In Figure 10 we show the fraction of background rejected as a function of primary energy for Milagro and a possible future instrument, HAWC (see "Future Directions" section). In this instrument, the entire physical area of the instrument is capable of muon detection ($\sim$20,000 m^2). As can be seen from the figure at $\sim$1 TeV roughly 95% of the background can be rejected and by 10 TeV nearly 99.5% of the background can be rejected.

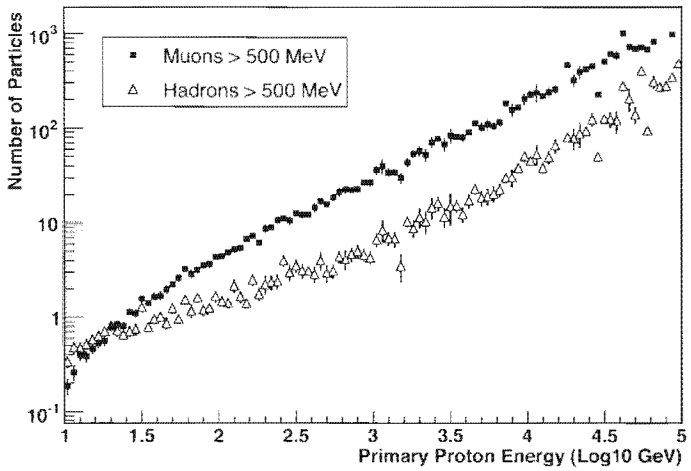

Figure 8. The average number of muons and hadrons to reach the ground as a function of primary proton energy. A minimum muon and hadron energy of 500 MeV was required and only particles falling within 100 m of the shower core were counted. The observation altitude was taken to be 5200 m above sea level.

3. Current EAS Arrays

There are three major EAS arrays in operation today: Milagro, the Tibet ASγ, and ARGO (Astrophysical Radiation with Ground-based Observatory). Table 1 summarizes the current generation of experiments along with the Cygnus and CASA-MIA arrays. Milagro (Figure 11) is located at an altitude of 2630 m above sea level and consists of a central water reservoir covering an area of ~4000 m^2, surrounded by an array of 175 water tanks covering an area of ~34,000 m^2 (the outrigger array). The central detector has dimesions 80m x 50m with a depth of 8m at the center. The reservoir is instrumented with 750 20cm photomultiplier tubes (PMTs) arranged in two layers. The top layer of 450 PMTs is under 1.4 meters of water and the bottom layer of 273 PMTs is under 6m of water. Both layers are on a 2.8m x 2.8m grid. The entire reservoir is enclosed with a light-tight cover. Each water tank has an area of 8m^2 and a depth of ~1m. They are instrumented with a single PMT that is mounted at the top looking down into a TYVEK lined water volume. The PMTs in the top layer and the outrigger array are used to reconstruct the direction of the primary gamma ray (or cosmic ray) to an accuracy of ~0.5 degrees. The bottom layer is used to discriminate against the background cosmic radiation. Air showers induced by hadrons contain a penetrating component (muons and hadrons that shower in the reservoir). This component results in a compact bright region in the bottom layer of PMTs (see [3] for details). A cut based on the distribution of light in the bottom layer removes 92% of the background cosmic rays while retaining 50% of the gamma ray events [10]. The trigger rate (before background rejection) is ~1700 Hz.

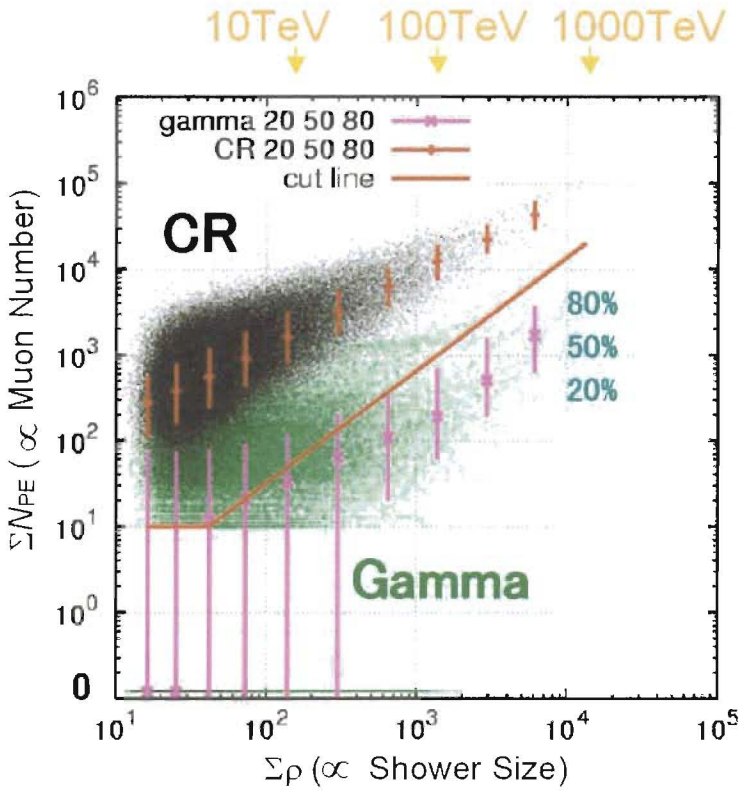

Figure 9. The number of detected muons that reach the ground as a function of the shower size for proton primary particles (black) and gamma-ray primaries (green). This figure was made using a Monte Carlo simulation of the Tibet+MD detector (described in more detail in the "Future Directions" section of this paper). A muon is defined as any buried detector with more than 10 detected photo-electrons within the Tibet+MD array. The minimum muon energy required to penetrate into the muon detector is 1.2 GeV. For a given shower size the the median number of detected muons is plotted and the error bars span the 20%-80% range of the distribution in the number of detected muons. For reference the average energy is indicated for three values of the shower size. Figure courtesy of Masato Takita.

Tibet ASγ (Figure 12) is a more traditional scintillator array located at an altitude of 4300m a.s.l. The detector has undergone significant upgrades over the past decade and is currently composed of 789 scintillation counters on a 7.5m grid. Each counter consists of a 0.5m^2 plastic scintillator viewed by a 5cm PMT. Each detector is covered with a 5mm sheet of lead. The total area enclosed by the array is 36,900 m^2. The trigger rate is $\sim$700 Hz and the angular resolution is 0.9 degrees.

The ARGO detector, Figure 13, is also located at the Yangbajing cosmic-ray observatory in Tibet. ARGO is a dense sampling array with 92% sensitive area over a 5,772 m^2 area and a total area of 11,000 m^2. The particle detectors in ARGO are resistive plate chambers (RPCs) - a parallel plate gas chamber. In ARGO each RPC

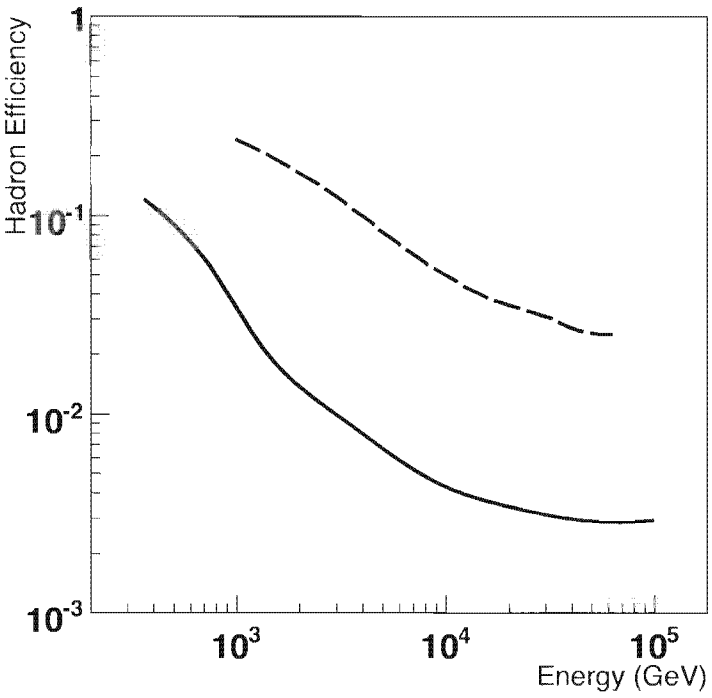

Figure 10. The fraction of the cosmic-ray background retained as a function of energy for the Milagro detector (dashed line) and a possible future instrument (solid line), HAWC (see below). Figure courtesy of Andrew Smith.

is composed of 10 pads each of which contains 8 detector strips. The spatial resolution is determined by the geometry of the strips and is 6.7 cm in one direction and 62 cm in the perpendicular direction. The time resolution of the RPCs is about 1 ns, similar to that of scintillation counters. The RPCs are arranged in groups of 12 (a cluster) and there will be a total of 154 clusters in the complete detector. As of the summer of 2007 there were 130 clusters operational covering an area of $\sim$5800 m^2 [5]. Since the detectors are thin there is no possibility to distinguish the passage of muons, however the ARGO collaboration expects to utilize the fine spatial resolution and dense sampling to distinguish air showers generated by gamma rays from those generated by hadronic cosmic rays. With an angular resolution of $\sim$0.5 degrees and a median energy of triggered gamma rays below 1 TeV ARGO should have the sensitivity to detect the Crab Nebula at 10 standard deviations in one year of observation without background rejection and 15σ with its background rejection capabilities.

Both Milagro and ASγ have conclusively demonstrated their sensitivity with detections of the Crab Nebula. ASγ has reported two independent detections of the Crab Nebula. In data taken between 1996 and 1999 they reported a 5.5σ detection with a less sensitive instrument, the HD array [9]. With the Tibet-III detector they report a 4.8σ detection with 1.5 years of running time [8]. This sensitivity on the Crab

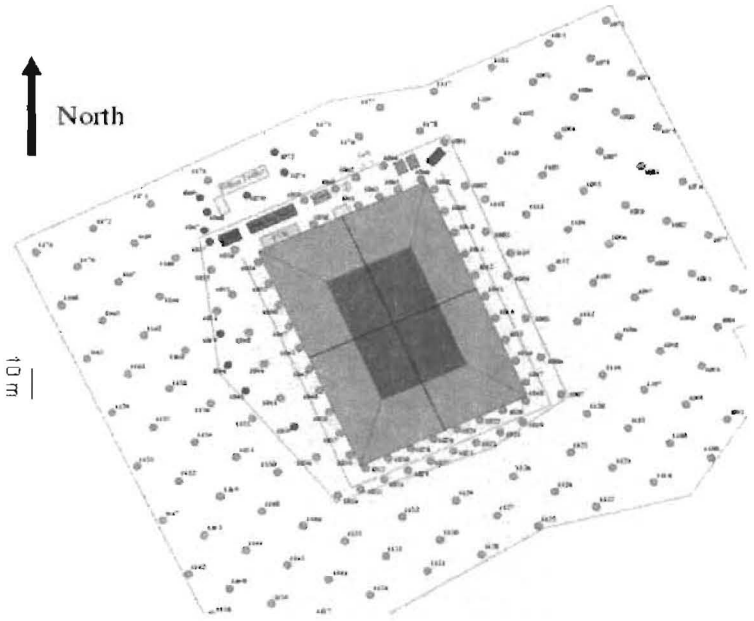

Figure 11. A schematic view of the Milagro telescope. The outrigger tanks are shown surrounding the central water reservoir.

Nebula ($4\sigma/\sqrt{yr}$) is comparable to that of the Milagro detector before the construction of the outrigger array. Milagro now reports a sensitivity of $\sim 8\sigma/\sqrt{yr}$ with the outrigger array [10]. The ARGO detector has reported a preliminary detection of both the Crab Nebula and Mrk 421 [5]. However, at the time of this report there remain outstanding issues related to the overall pointing of the instrument, and it is impossible to measure the sensitivity of ARGO using these measurements. (For both the Crab Nebula and Mrk 421, the reported excesses are not centered upon the known source locations. Therefore, the true significance of the observation is not known. Simply taking the largest excess in the region of the source would lead to an over-reporting of the sensitivity of the detector. Similarly, with the suspicion of a systematic pointing error, taking the observed significance at the known source location would underestimate the sensitivity of the detector.)

4. Sky Surveys

One of the primary motivations for a synoptic instrument is to perform an unbiased sky survey. Both Milagro [15] and Tibet [16, 17] have surveyed the Northern sky for point sources of TeV gamma rays. (For details of various methods employed for estimating the background and assigning statistical significances to observations see [18].) Figure 14 shows a more recent map made by the Milagro collaboration [19]. The data in this map was taken over a 6.5 year period from July 2000 to January 2007. The median

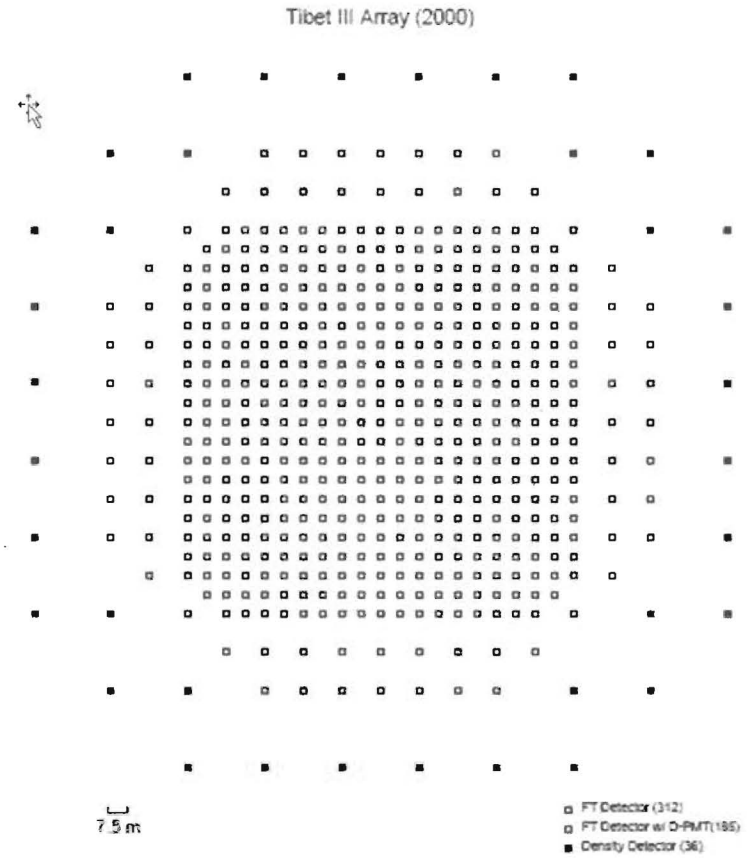

Figure 12. A schematic of the Tibet ASγ array.

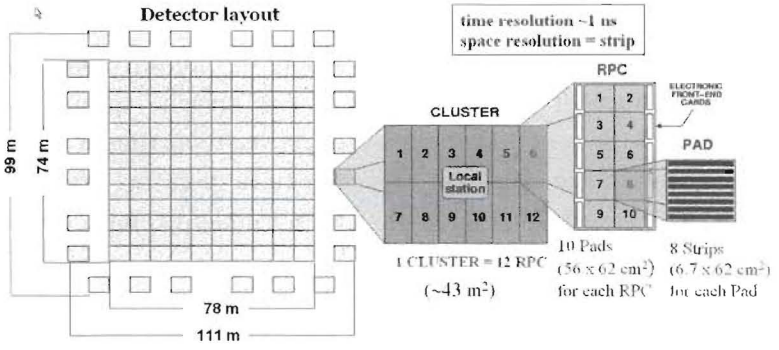

Figure 13. A schematic of the ARGO detector.

energy of detected gamma rays in this map was 12 TeV. There are several noteworthy features in the map. With statistical significance of 15 standard deviations, the Crab Nebula is the most significant point source detected by Milagro. The bottom panel of Figure 14 clearly shows gamma-ray emission in the region near the Galactic equator.

Table 1. Extensive Air Shower Arrays for VHE γ-rays

Experiment (site)	Location[a] atm. depth	Array Area m^2	N[b]	μ[c] m^2	Event Rate s^{-1}	Operation
CASA-MIA (Dugway, Utah)	40.2°N, 112.8°W 870 g/cm^2	230,400	1089	2,500	20	1991-1996
CYGNUS (Los Alamos, NM)	35.9°N, 106.3°W 800 g/cm^2	86,000	204	120	5	1986-1996
Milagro (Jemez Mtns, NM)	35.9°N, 106.7°W 750 g/cm^2	40,000	898[d]	2,400	1700	2000-2008
ASγ (YangBaJing, Tibet)	30.1°N, 90.5°E 600 g/cm^2	53,000	497	NA	700	1990-present[e]
ARGO (YangBaJing, Tibet)	30.1°N, 90.5°E 600 g/cm^2	11,000	1848[f]	NA	2000	2007-present

[a] geographical latitude and longitude of the observation site
[b] number of detector elements
[c] area of muon detector
[d] number of PMTs. See text for detailed detector description.
[e] configuration varied. The latest configuration is given.
[f] number of RPC detectors. See text for detailed detector description.

This will be discussed in detail below. The only object visible outside of the Galaxy is the active galaxy Mrk 421, this is also true of the results from the Tibet ASγ detector [17]. Mrk 421 lies at a distance of $\sim$120 Mpc from Earth and was first detected at TeV energies by the Whipple telescope [20]. While there are many other known AGN that emit TeV gamma rays, the high-energy threshold of the current generation of EAS arrays make them difficult to detect using this technique. (This is due to the absorption of TeV gamma rays via interactions with the extra-galactic background light (EBL) [21] that pervades the universe.)

5. Galactic Plane Survey

The Milagro sky survey shows clear evidence for TeV gamma-ray sources localized to the Galactic plane. Figure 15 shows a more detailed view of the Milky Way in gamma rays with a median energy of 20 TeV. The range of Galactic longitude visible is limited by the latitude of the Milagro observatory and a requirement that events fall within 45 degrees of zenith to be considered in the analysis. The boxes mark the locations of EGRET sources (from the 3rd EGRET catalog [22]) and the crosses mark the locations of GeV gamma-ray sources identified by EGRET [23]. The sensitivity of this survey is between 3 and 6 $\times$ 10^{-15} TeV^{-1} cm^{-2} s^{-1} [24] at 20 TeV. There are a total of 8 regions with an excess above background of over 4.5 standard deviations (including the Crab Nebula) [note: see Figure 16 for the location of C2, which is not shown in Figure 15]. Table 2 gives relevant information for these 8 sources [10]. Those regions with a

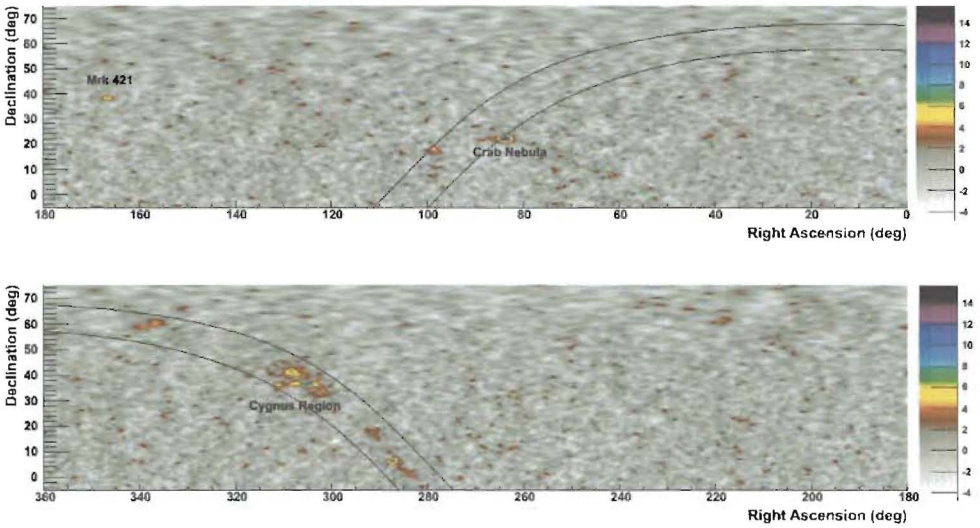

Figure 14. Map of the Northern hemisphere in TeV gamma rays (the Milagro collaboration) with 2.1 degree smoothing (optimized for point sources). The black lines are drawn at ± 5 degrees around the Galactic plane. The color scale is standard deviations.

Object Name	Coordinates	Significance	Flux ($\times 10^{-15}$TeV^{-1}cm^{-2}s^{-1})	Extent
Crab Nebula	184.5, -5.7	15.0	10.9$\pm$1.2	...
MGRO J2019+37[a]	75.0, 0.2	10.4	8.7 $\pm$1.4	1.1 $\pm$ 0.5
MGRO J1908+06[b]	40.4, -1.0	8.3	8.8 $\pm$ 2.4	$<$ 2.6
MGRO J2031+41	80.3, 1.1	6.6	9.8 $\pm$ 2.9	3.0 $\pm$ 0.9
C1	77.5, -3.9	5.8	3.1 $\pm$ 0.6	$<$ 2.0
C2	76.1, -1.7	5.1	3.4 $\pm$ 0.8	...
C3	195.7, 4.1	5.1	6.9 $\pm$ 1.6	2.8 $\pm$ 0.8
C4	105.8, 2.0	5.0	4.0 $\pm$ 1.3	3.4 $\pm$ 1.7

Table 2. Results of the Milagro Galactic Plane Survey. Locations are given in Galactic coordinates (longitude, latitude), the significance is pre-trial, the flux is at 20 TeV and the extent is the diameter of the object measured in degrees.
[a] Confirmed by the Tibet ASγ detector [25]
[b] Confirmed by the H.E.S.S. telescope [31]. The Tibet ASγ collaboration observes a 4.3σ excess at this location [17]

post-trial significance (the number of trials associated with this survey of the Galactic Plane were calculated using a Monte Carlo simulation of the search) over 5 standard deviations are identified as new sources and given an MGRO JXXXX+XX designation. Otherwise the region is called a source candidate and labeled Cn. We discuss the details of each source below.

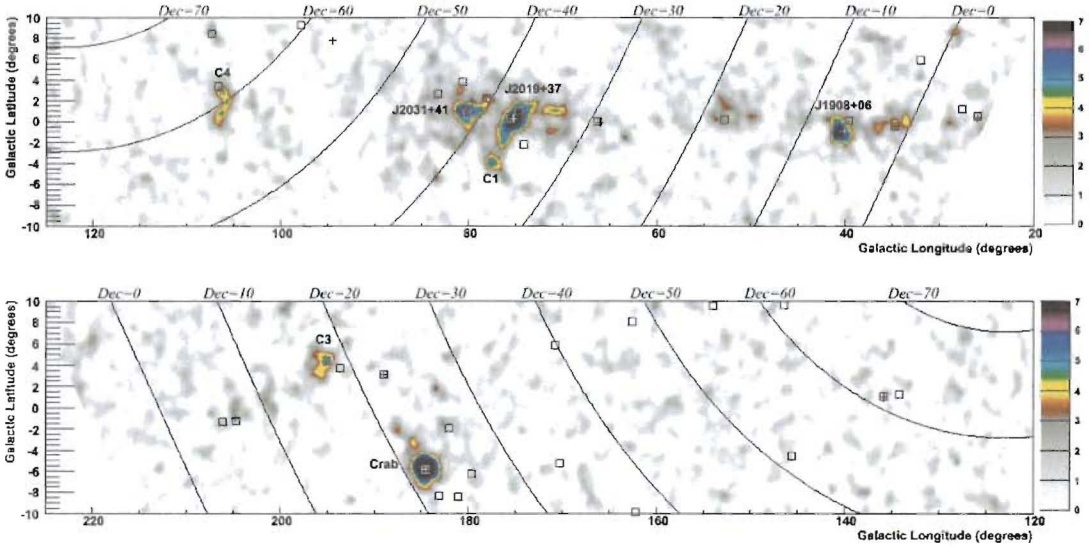

Figure 15. The Galaxy in TeV gamma rays from Galactic longitude 20 degrees to 220 degrees and Galactic latitude from -10 degrees to 10 degrees. The image is the culmination of a seven year exposure by the Milagro instrument. The color scale shows the statistical significance of the observed excess (over the cosmic-ray background) at each point. Crosses mark the location of GeV sources and boxes mark the location of sources in the 3EG catalog. Locations marked as C1,C3, & C4 are candidate sources as determined by Milagro and the three locations marked as JXXXX+YY are sources discovered by Milagro. To improve the clarity of the figure significances above 7 standard deviations are shown as black and those below 3 standard deviations are shown as a monochrome.

There are several noteworthy features of these sources all of which are consistent with the interpretation that these new TeV sources are pulsar wind nebula (PWN).

- This is a high-energy survey, therefore these sources must have relatively hard spectra. The differential spectral index that connects these measurements with EGRET measurements (when there is an EGRET counterpart) is -2.3.
- Many of the sources are extended, with large extents by TeV standards.
- There is a strong correlation between these sources and the EGRET GeV catalog. Excluding the Crab Nebula there are 13 GeV sources within this survey area. Five of the seven sources and source candidates lie within a 3x3 degree box centered on the EGRET GeV sources. The chance probability of such an occurrence is 3×10^{-6}.

5.1. Point and Extended Sources

The Cygnus Region: The region spanning Galactic longitude 70 and 85 degrees is known as the Cygnus Region after the eponymous constellation located in the area. From the Earth this direction is along the spiral arm of the Galaxy in which we reside. Therefore we are looking into a large column density and at relatively nearby objects

(~1-2 kpc). The region contains several potential cosmic-ray acceleration sites - Wolf-Rayet stars [26], OB associations [27], and supernova remnants [28]. In addition there is an unidentified TeV source, TeV J2032+413 [29] and 4 GeV sources [23]. Milagro has identified two definite sources and 2 source candidates in this region. Figure 16 shows the TeV emission from the Cygnus Region (as observed by Milagro), along with the locations of hotspots identified by the Tibet ASγ array.

MGRO J2019+37: The brightest TeV source in the Cygnus Region is MGRO J2019+37 [10, 24]. As seen from Figure 16 this source has also been detected by the Tibet ASγ observatory (T1 in the figure). The position of the TeV MGRO J2019+37 is consistent with PWN G75.2+0.1 and with the blazar B2013+370 [30]. Given the angular size of the TeV source and the high-energy emission it is unlikely that the blazar is the TeV source.

MGRO J2031+41: The location of MGRO J2031+41 is consistent with the previously reported position of TeV J2032+413 discovered by the HEGRA collaboration [29]. However the flux at 20 TeV is about a factor of three higher than a straightforward extrapolation of the flux of TeV J2032+413 measured by HEGRA (up to 10 TeV). Thus, it is likely that this is a new source. The Tibet array has also detected emission from this source (T2 in Figure 16).

MGRO J1908+06: The H.E.S.S. collaboration has performed follow-up observations of this source and report a significant detection [31]. H.E.S.S. measures a very hard spectrum, with a differential spectral index of -2.08$\pm$0.1$_{stat}$ $\pm$ 0.2$_{sys}$ between 400 GeV and 30 TeV. The source size measured by H.E.S.S. is 0.21 degrees (Gaussian width), consistent with the Milagro upper limit on the source extent. The flux at 20 TeV as measured by H.E.S.S. is in excellent agreement with the flux reported by Milagro. Because of the low declination of this source (and subsequently the large zenith angle of the Milagro observations) the actual median energy of the Milagro detection is ~50 TeV. MRGO J1908+06 may be the highest energy gamma-ray emitter observed to date and is a candidate for a cosmic-ray accelerator. A more detailed analysis of the energy spectrum - in particular at the highest possible energies, >100 TeV, is needed.

C1: Source candidate C1 is the only source (excluding C2) that is not coincident with a GeV source (or any EGRET source). It is far enough from the Galactic plane (~4 degrees) that the Galactic diffuse emission is small at TeV energies. The apparent confirmation of the source by the Tibet observatory (T3 in Figure 16) seems to indicate that this is a true TeV source. Follow-up observations by the VERITAS instrument will be crucial for resolving the nature of this source.

C2: Source candidate C2 is part of a complicated region (see Figure 16. With a large matter density the contribution from a diffuse component is expected to be large and the nearby extended source J2019+37 (with a poorly measured morphology) may also contribute to the observed excess. It is not clear that there is a new point or extended source of TeV gamma rays at this location. Given the low statistical significance of the detection and the complications of the gamma-ray background in the region it is likely that this excess is due to a statistical fluctuation of the gamma-ray background.

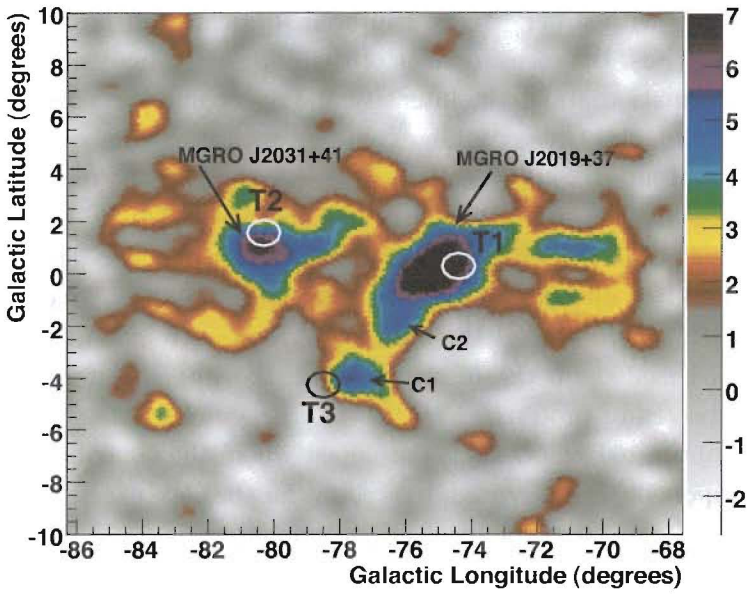

Figure 16. The Cygnus Region as seen in TeV gamma rays. The color scale represents observations form the Milagro observatory. The circles marked T1, T2, T3 are the locations of hot spots in the region detected by the Tibet ASγ observatory. The significances of these hotspots (as reported by Tibet ASγ) are T1= 5.8σ, T2=3.8σ, and T3=4.1σ.

C3: This source candidate is coincident with the Geminga radio-quiet pulsar, the second brightest GeV gamma-ray source in the sky. At ~170 pc from earth Geminga would be the closest TeV source to earth. The pulsar period is 0.237 seconds and is seen in the x-ray and gamma-ray bands. Geminga is believed to have originated in a supernova explosion about 340,000 years ago. The angular size of the TeV object measured by Milagro, 2.8±0.8 degrees, is significantly larger than that observed at x-ray wavelengths, where a 20" tail is observed [32]. Given the distance to Geminga the TeV source diameter would be ~8±2.3 pc, consistent with other PWN detected in the TeV band [33, 34].
Source Candidate C4: This region is coincident with the Boomerang PWN and a GeV source. The TeV emission is clearly extended and the significance of the observation increases to 6.3 standard deviations (pre-trial) in a 3x3 degree bin. The >100 MeV emission detected by EGRET has a very similar extended structure to that observed by Milagro at 20 TeV.

5.2. Diffuse TeV Gamma-Ray Emission

In addition to the sources discussed above Figure 15 shows the presence of a diffuse gamma-ray flux from the Galaxy, especially near the Cygnus Region and at lower Galactic longitude (near MGRO J1908+06). This diffuse emission is expected to be due

to the interaction of cosmic-ray nuclei with matter and inverse Compton interactions of high-energy electrons with lower energy (infrared, optical, and cosmic microwave background) photons. Thus, the measurement of the diffuse gamma-ray emission from our Galaxy yields information about the intensity and spectrum of cosmic ray protons and electrons throughout the Galaxy. Lower energy measurements by the EGRET showed clear evidence of an excess (over predictions based upon the measured matter density and the local cosmic-ray intensity and spectrum) above 1 GeV [35]. Explanations of this GeV excess range from the annihilation of dark matter particles [36] to a varying cosmic-ray spectrum and/or intensity across the Galaxy [37, 38, 39]. A model has been developed (GALPROP [37]) to predict the diffuse gamma-ray emission throughout the Galaxy, the model is based upon the matter density, the interstellar radiation field, and the cosmic-ray spectra of protons, electrons, and heavy elements. To account for the GeV excess an "optimized" model was developed where the contribution from the inverse Compton component was increased, to account for the GeV excess. (The original GALPROP model is referred to as the conventional model below.) While this increase is relatively small at GeV energies, it predicts that at TeV energies the inverse Compton component dominates over the pion component. (The pion component arises from the interaction of hadronic cosmic rays with matter.) Therefore, if this interpretation is correct, measurements of the diffuse gamma radiation at 10 TeV are indicative of the $\sim$100 TeV electron spectrum at distant locations within the Galaxy.

Figure 17 [40] shows the diffuse TeV gamma-ray flux and the predictions of both the conventional and optimized GALPROP models. The median energy of the Milagro detection is 20 TeV. The data shown in the figure have had the contributions from the sources discussed above removed, and thus represent the diffuse flux (in the absence of other as yet unresolved sources). Note that even the optimized version of GALPROP under predicts the TeV flux by a factor of 2.7 in the Cygnus Region. The excess above the GALPROP prediction has a statistical significance of roughly 3 standard deviations. This excess could be explained by the existence of a cosmic-ray accelerator within the Cygnus Region, which would lead to a harder spectrum of cosmic rays within this region and therefore a larger flux of high-energy gamma rays. This explanation is interesting in light of the recent results from the ACE CRIS instrument [41]. This direct measurement of the isotopic abundances of the local cosmic rays at lower energies ($\sim$100 MeV/nucleon), indicates that roughly 20% of the Galactic cosmic rays originate from Wolf-Rayet stars (typically found in OB associations). Alternatively, the excess could be explained by unresolved point sources of TeV gamma rays that may lie within the Cygnus Region. The resolution of this question awaits follow-up observations by the VERITAS gamma-ray telescope, which should have the sensitivity to detect as yet unresolved gamma-ray sources (though a measurement of the diffuse emission in this region will be difficult for VERITAS).

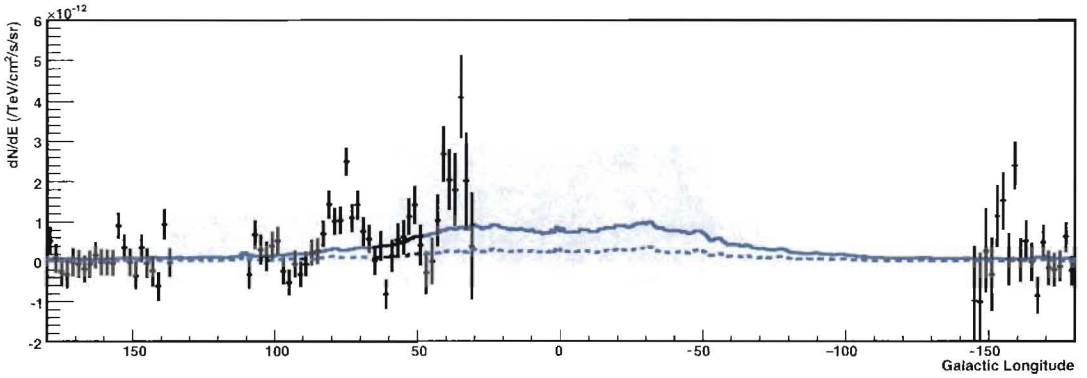

Figure 17. The longitudinal profile of the Galactic diffuse emission of TeV gamma rays measured by the Milagro observatory [40]. The solid line shows the prediction of the "optimized" GALPROP model (increased inverse Compton component to fit EGRET data) and the dashed line shows the prediction of the "conventional" GALPROP model (cosmic-ray intensity and spectrum assumed to be the same as measured at earth). Note that even the optimized model under predicts the TeV measurement in the Cygnus Region.

6. Anisotropy of the Cosmic Radiation

While several groups have previously reported measurements of cosmic-ray anisotropy (see [42] for a review), these measurements have been one-dimensional, i.e. anisotropy as a function of right ascension. Recently, this situation has changed and current experiments have the statistical power to make quasi-2-dimensional maps of the anisotropy of cosmic rays in the energy range from 1-100 TeV. (The maps are not truly 2-dimensional since they do not have the ability to measure a declination dependent anisotropy. instead they are a series of 1-dimensional maps that give the anisotropy as a function of right ascension versus declination. This is due to the fact that, to date, the data analyses have relied upon the rotation of the earth to determine the relative response of the instruments as a function of local coordinates [43].) The Tibet ASγ observatory has produced the first such map [44], see Figure 18. There are two striking features of this map: the large deficit near a right ascension of 180 degrees (Region I in the figure) and the excess between right ascension 50 and 70 degrees (Region II in the figure). The cosmic-ray intensity in the region of the deficit is 0.998 that of the average cosmic-ray intensity and in the region of the excess about 1.003 times that of the average cosmic-ray intensity. The direction of the deficit is the direction perpendicular to the Galactic plane. Despite their ability to observe these anisotropies, the Tibet group failed to detect the Compton-Getting effect associated with the motion of the Sun in the Galaxy. First predicted by Compton in 1935 [45] this effect is due to the earth's motion through a cosmic-ray gas at rest with respect to the Galaxy. The non-observation of the effect is evidence that the cosmic rays co-rotate with the matter in

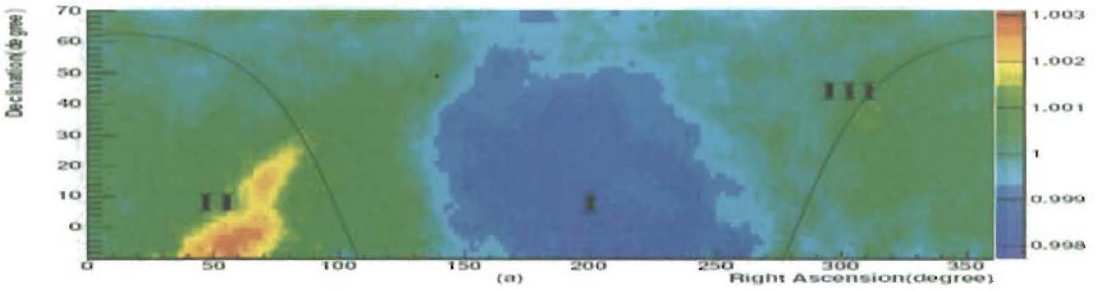

Figure 18. The anisotropy in the cosmic radiation as measured by the Tibet ASγ observatory. This is the first two-dimensional map of high statistical significance of the cosmic-ray anisotropy. Region III is the Cygnus Region and the observed excess in that direction is consistent with the gamma-ray flux measured by Milagro in that direction.

our spiral arm of the Galaxy. The direction of the excess in Region II is consistent with the "tail-in" region of the heliosphere, the direction of open magnetic field lines (opposite to the direction of motion of the Sun through the local interstellar medium). Also evident in Figure 18 is a smaller excess in Region III. This region is the Cygnus Region and given the observations discussed above it is likely that the observed excess is due to gamma rays from the Cygnus Region, the fractional excess observed by the Tibet ASγ is consistent with the gamma-ray flux reported by Milagro from the entire region.

The Milagro collaboration has also searched for large-scale and intermediate scale anisotropies in the cosmic-ray arrival directions. The large-scale anisotropy results from Milagro are consistent with those reported by Tibet [46, 47], however Milagro has also observed that the amplitude of the anisotropy is time-dependent (the phase of the anisotropy does not change with time). Figure 19 shows the amplitude of the anisotropy as a function of the year of the observation. It should be noted that the beginning of the observations (2000) was during solar maximum and the end of the observations (2007) occurred during solar minimum. This observation implies that the more recent data represent the true amplitude of the anisotropy of the Galactic cosmic rays. At energies near 1 TeV the heliosphere can affect the propagation of cosmic rays [48, 49], though at much higher energies one does not expect an influence from the heliosphere. Milagro has also measured the energy dependence of the anisotropy and find that the amplitude is a maximum near 4 TeV and persists to at least 100 TeV. The anisotropy at the higher energies may be due to the distribution of nearby (<1 kpc) young (<50 kyr) supernova remnants and the diffusion of cosmic rays [50, 51].

A search for intermediate scale anisotropy has uncovered several puzzling features. A 2-dimensional plot of the intermediate scale anisotropy of the cosmic radiation is shown in Figure 20 [52]. The smoothing scale for this analysis was 10 degrees. There are two notable localized excesses: Region A, near a right ascension of 70 degrees,

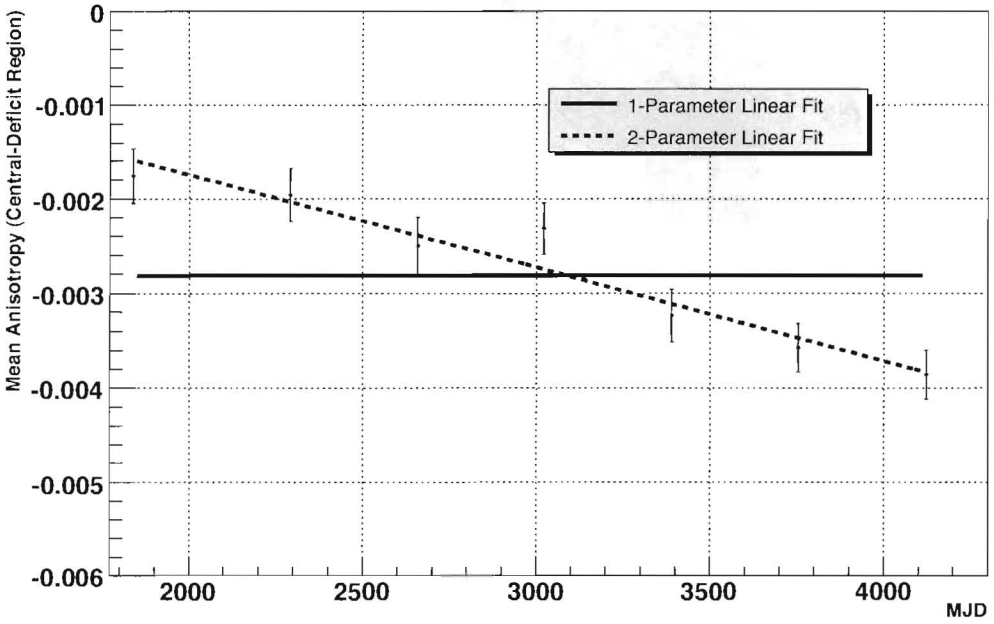

Figure 19. The amplitude of the large scale anisotropy in the cosmic radiation as a function of modified Julian date minus 50,000. The data was taken with the Milagro detector. An x-axis label of 2000 corresponds to April 1, 2001 and the label 4000 is September 22, 2006.

and region B, the large arc near a right ascension of 130 degrees. With its ability to distinguish gamma-ray induced EAS from hadronic EAS [3], the Milagro data have been used to conclusively demonstrate the hadronic nature of these excesses [52]. A coarse estimate of the energy spectrum of Region A has been made using the Milagro data. The excess has a harder spectrum than the cosmic-ray background and disappears above about 10 TeV. Given that the Larmor radius of a 10 TeV proton in the local magnetic field (2μGauss [53]) is roughly 0.005 pc and the decay length of a 10 TeV neutron is only 0.1 pc, it is difficult to understand the phenomena that may be the cause of the observed excesses, though several explanations have been proposed [54, 55].

7. Future Directions

Given the success of the Milagro and Tibet observatories it is natural to consider future improvements to all-sky TeV gamma-ray observatories. A future EAS array could be completed in 3-5 years and it must be placed in the context of that time period. This includes not only gamma-ray instruments, but neutrino and ultra-high-energy (UHECR) telescopes. The strengths and weaknesses of an EAS array should be considered relative to these other instruments and a clear rationale developed for further development and

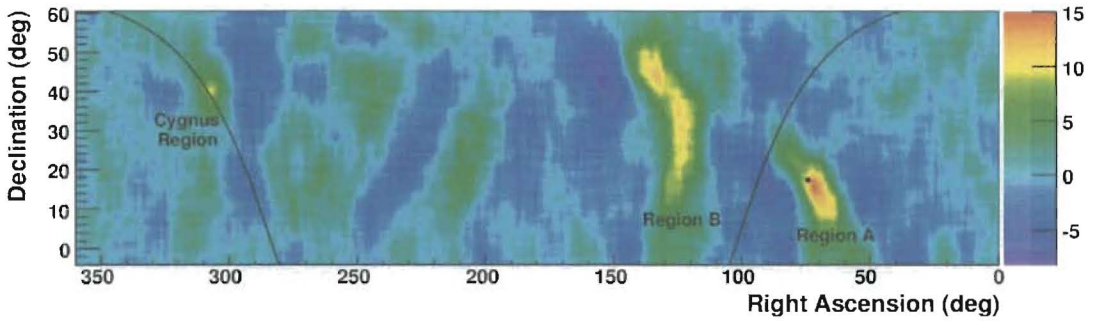

Figure 20. The anisotropy in the local cosmic ray flux over intermediate scales (~10 degree smoothing length). The color scale shows the statistical significance of the excess in each 10×10 degree bin centered at the given right ascension and declination. The excess is measured with respect to a local average cosmic-ray flux within about 15 degrees of the location. The fractional excess in Region A is roughly 6×10^{-4} and in Region B roughly 4×10^{-4}.

fielding of such an instrument.

GLAST [56, 57, 58] will have been taking data for 3-5 years and it will have discovered several thousand ~100 MeV gamma-ray sources and mapped the Galactic diffuse emission up to at least 100 GeV. The current generation of IACTs (MAGIC [59, 60], H.E.S.S. [61], and VERITAS [62]) will have been operating for this entire time and they will have searched for (and detected) >100 GeV gamma-ray emission from many of the GLAST sources. The next generation of IACT (such as the European Cherenkov Telescope Array effort or the U.S. based Advanced Gamma-Ray Imaging System effort), with roughly an order of magnitude better sensitivity than current IACTs, may be under construction. The IceCube neutrino detector will be complete and operating. It is likely that they will have discovered several cosmic neutrino sources, and therefore acceleration sites of hadronic cosmic rays. With respect to UHECRs, recent results from the High Resolution Fly's Eye Experiment, demonstrating the existence of the GZK suppression above $10^{19.6}$eV [63], shows that the UHECR sources must be quite close to Earth, within ~100 Mpc and results from the Auger experiment indicate that the directions of the highest energy UHECRs maybe correlated with nearby active galaxies [64]. Searching for gamma-ray counterparts to UHECR sources should be a high priority for the field. The Auger collaboration is planning to construct a very large array (~ 30,000 km^2) in the northern hemisphere, which may well discover point sources of UHECRs.

7.1. Complementarity of EAS and IACT Arrays

Before discussing the role of future EAS arrays one should consider their relevance given the enormous success of the IACT technique. In the optical band there are large

	EAS Array	IACT	Relevant Physics
Aperture	~2 sr	~4 msr	Surveys, Extended Objects, Diffuse Emission, Transient Phenomena
Duty Factor	~100%	~10%	Highest Energies, Acceleration Models
Energy Resolution	~50%	~10%	Dark Matter, Source Spectra
Angular Resolution	~0.5°	~0.1°	Source Morphology
Median Energy	~1 TeV	~100 GeV	Extragalactic (IACT), High-Energy (EAS)
DC Sensitivity[a] E·F(>E)	10^{-13} @ 10 TeV	10^{-13} @ 700 GeV	Surveys
Transient Sensitivity[a]	2×10^{-10} @ 500 GeV	2×10^{-12} @ 500 GeV	Rapid Flaring

Table 3. Comparison of EAS and IACT arrays. The values given are characteristic values and are dependent upon the exact instrument under consideration. The DC sensitivity is given for a point source with a Crab-like spectrum. For an IACT the sensitivity given is based upon a 50 hour observation by H.E.S.S. or VERITAS. For an EAS array it is given for a 5-year period for HAWC (see below). The next generation of IACTs will have roughly an order of magnitude improved sensitivity. The transient sensitivity is given for a 10 minute observation for both types of instruments. Because of the absorption by the EBL the transient sensitivity of an EAS array is given at an energy of 500 GeV. At an energy of 10 TeV the flux sensitivity is about an order of magnitude smaller.
[a] units are TeV $cm^{-2}sec^{-1}$.

telescopes such as Keck [68], that are sensitive to extremely dim objects and wide-field cameras such as ROTSE [66] or RAPTOR [67] that have been highly successful in studying the transient universe. In this case there is a trade-off between aperture and sensitivity. The situation is similar in the TeV energy regime. The IACTs are pointed instruments with a relatively small field-of-view (~4 msr), and they only operate for ~10% of the time, yet they are sensitive to very low flux levels. On the other hand EAS arrays have a substantially poorer instantaneous sensitivity, yet they have a very large field-of-view (~2 sr) and operate continuously. The strengths of an EAS array derive from these two characteristics. In Table 3 we give the relative strengths and weaknesses of the two techniques and the physics that is most relevant to each technique.

IACTs are excellent instruments for studying known or suspected sources, and performing deep surveys of limited regions of the sky (such as the Galaxy). Their unsurpassed instantaneous sensitivity enables them to quickly measure low fluxes, enabling them to detect the fastest flares from AGN or emission from gamma-ray bursts (though not the prompt emission, since they must re-direct the telescope pointing after receiving an external alert). IACTs have a low energy threshold enabling them to view distant AGN, where the source spectra are attenuated at higher energies by the EBL

([21], and references therein). The excellent angular resolution of IACTs enables them to map extended Galactic sources, the morphology of which can then be compared to x-ray and other measurements. The excellent energy resolution of IACTs makes them sensitive to the annihilation of dark matter and allows for detailed study of the energy spectra of cosmic acclerators. The two weaknesses of an IACT are the field-of-view (typically ~4 msr) and the available duty cycle, ~10%.

Complementing these attributes, an EAS array continuously views the entire overhead sky. The strengths of an EAS array (sensitivity to transient phenomena, the highest energy gamma rays, and sensitivity to extended objects) derive from this capability. While it is obvious how these characteristics enable the study of transient phenomena, in particular, TeV emission that is coincident with (or even prior to) emission at other wavelengths, the remaining strengths warrant further discussion.

We have seen that at high energies an EAS array can operate in an essentially background free (or very low background) regime. In such a mode the sensitivity of an instrument is proportional to the inverse of the effective area multiplied by the time on source. The proportionality constant is the number of detected gamma rays required to claim a signal. Because an EAS array views every source for ~1400 hours per year (as compared to 10-100 hours for selected sources for an IACT) and has comparable effective area at high energies, it will be 14-140 times more sensitive than an IACT - allowing one to extend the energy reach by a factor of 4-12 (for source spectra $dN/dE \propto E^{-2}$). This sensitivity to the highest energy gamma rays is important for studying potential cosmic-ray accelerators within our Galaxy, where one expects any spectral cutoff to occur at high energies.

The sensitivity of an instrument to an extended source is approximately equal to its point source sensitivity if the source is smaller than the angular resolution of the instrument. For larger sources the sensitivity is degraded by the ratio of the source size to the angular resolution of the instrument [69]. This is simply due to the fact that the background level is proportional to the square of the source size (since the background must be integrated over the entire source) and therefore the fluctuations in the background level are proportional to the source size. Therefore, if a source has a radius of 1 degree an instrument with an angular resolution of 0.1 degrees, will require 10 times the flux from that source to achieve a detection of similar statistical significance as would be achieved from a point source. Because EAS arrays have worse angular resolution than IACTs, their sensitivity does not begin to degrade until the source size is quite large (~5 times larger than for an IACT, see Table 3. In addition to this effect, an IACT suffers in its ability to characterize the background for the largest sources, i.e. those larger than the field-of-view the instrument. An EAS array, with its extremely large field-of-view can characterize the background for and detect even the largest sources.

7.2. Role of a Future EAS Array

We are now prepared to answer the question posed near the beginning of this section, what is the role of a future EAS array?

- Very-high-energy gamma-ray sky survey. While GLAST will discover thousands of sources, an IACT system can not observe thousands of regions of the sky. Thus, it will be left to EAS arrays to perform search for TeV counterparts to all of the GLAST sources and to perform a complete survey of the TeV sky.
- Mapping the Galactic diffuse gamma-ray emission. One of the largest TeV sources in the sky is the Milky Way. The next generation EAS array should have sufficient sensitivity to map this emission in regions comparable in size to the capabilities of GLAST, and the ability to obtain spectral information in the TeV band. These observations would allow one to probe the high-energy electron and cosmic-ray spectra throughout the Galaxy.
- Measuring the highest energy gamma rays from Galactic sources. These measurements will allow us to determine the limits of the acceleration processes occurring within our Galaxy and search for potential sites of cosmic-ray acceleration.
- Transient phenomena - active galactic nuclei. While IACTs will make detailed measurements of many flares from AGN, most of these observations will be triggered by instruments operating at other wavelengths (GLAST, x-ray or optical instruments). EAS arrays could determine the fraction of "orphan" flares (those that only exhibit TeV emission), and measure the flaring rates (duty factor) at TeV energies of a large number of AGN.
- Transient phenomena - gamma-ray bursts. IACTs will be very sensitive to delayed emission from gamma-ray bursts. To detect the prompt (or early) emission one requires an EAS array.
- Transient phenomena - IACT alert system. While GLAST and x-ray satellites will provide a plethora of transient phenomena for IACTs to follow-up, the list of objects to observe may well exceed the time availability of these instruments. A TeV transient alert system, based on an all-sky monitor can narrow the list of candidates for IACTs to observe. In addition, the next generation EAS array will likely be operating after the GLAST mission is complete and IACT arrays will need an all-sky monitor to maximize their scientific return.
- Surreptitious discovery. It is nearly certain that the most exciting discoveries from an all-sky instrument will not be on the above list. An all-sky instrument allows one to discover objects that one was not searching for or expecting to detect.

To understand the complementarity of EAS an IACT arrays we consider two examples: potential UHECR sources, and neutrino sources. If a source of high-energy cosmic neutrinos is discovered, an IACT is best suited to study the source in detail, determine its morphology and energy spectrum. However, because the neutrino flux is low ($\sim$10 events/year) and the determination that the object is a neutrino source will

be made after a lengthy observation period, an IACT will not be able to determine if the neutrino emission occurred during states of enhanced gamma-ray emission. An EAS array, with sufficient sensitivity would be able to search its past data and determine if there is a correlation between the gamma-ray and neutrino emission. In the case of UHECR sources, if there is a single or very few identified sources of UHECRS, an IACT array is best able to study the individual sources. On the other hand, if there is only a statistical correlation between UHECR events (as is the case with the recent result from the Auger collaboration [64]) and a class of sources, an EAS array will be better able to determine if the same correlation holds in gamma rays.

7.3. Possible Future EAS Arrays

The above physics goals can be separated into two categories: those that require a high sensitivity at extremely high energies (near and above 100 TeV) and those that require the lowest possible energy threshold - or significant sensitivity at low energies (i.e. near 100 GeV). The latter goal requires the highest possible altitude for the observatory and a dense array, sensitive to all electromagnetic particles (electrons, positrons, and gamma rays). The former goal requires the largest possible enclosed area and excellent background rejection at the highest energies. The Tibet+MD collaboration is seeking to build just such an array as an extension of the existing Tibet ASγ detector at the Yangbajing Observatory in Tibet, China. The HAWC collaboration [70] is seeking to build a detector optimized for lower energies at Sierra Negra in Mexico.

HAWC is a water Cherenkov extensive air shower array at the Sierra Negra site in Mexico. The altitude of the observatory would be 4100 m above sea level. In addition to the increased altitude the response of HAWC will be further improved (relative to Milagro) by the optical isolation of each detection cell, and a factor of $\sim$10 increase in the size of the muon detection area. A schematic of HAWC is shown in Figure 21, it will be composed of 900 large water tanks, each 4.3 meters tall with a diameter of 5 m. The tanks will be instrumented with a single 8 inch PMT placed at the bottom, looking up at the water volume. The total area of the array will be 150m$\times$150m, with $\sim$75% active detection area. Figure 22 shows the effective area as a function of primary gamma-ray energy for HAWC (the effective area of Milagro is shown for comparison). The curves shown in the figure include the reduction in effective area due to the angular reconstruction (only events that are reconstructed within 1.2 degrees of their true direction are included) and the background rejection efficiency for gamma-ray events (only events that pass the background rejection criteria are included). Because of the larger area available for muon detection, HAWC will reject about an order of magnitude more background than Milagro (i.e. at 10 TeV HAWC will retain roughly 0.4% of the background whereas Milagro retains about 5% of the background), see Figure 10. The median energy of detected events would be $\sim$1 TeV.

As an example of how HAWC will extend the measurements made by GLAST to higher energies we consider the case of extragalactic transients: flares from active

galaxies or gamma-ray bursts. To properly understand the sensitivity of an EAS array to extragalactic phenomena one must account for the absorption of high-energy gamma rays due to interactions with the EBL. The optical depth of high-energy gamma rays can be parameterized as $\tau \sim z^{4/3}(E_{GeV}/90)^{3/2}$ [71], for redshifts between 0.1 and 2. Thus, at 1 TeV ~36% of the source flux a survives a distance of z=0.07, and about 20% of the source flux would survive to a redshift of 0.1. There are 65 known BL Lacs and nearly 5000 known AGN within a redshift of 0.1 [72]. (BL Lacs are radio loud active galaxies with their jets directed at the Earth.) These source populations represent a rich field for GLAST, HAWC, and current and future IACTs. Many of these BL Lacs will exhibit flaring activity. In addition, the results from the Auger collaboration and the observation of M87 by the H.E.S.S. collaboration [73], raise the possibility that there exist many AGN whose jets are not directed at the Earth yet emit detectable levels of VHE gamma rays. To study transient events from these objects and study AGN that are not BL Lacs, requires an all-sky instrument working in concert with IACT arrays, GLAST and x-ray instruments. In Figure 23 we show the sensitivity of GLAST to >10 GeV emission and HAWC to transient phenomena. This figure shows that HAWC is well suited to measure the high-energy component of GLAST transients into the >100 GeV regime. For example at the shortest timescales (less than 1000 seconds) HAWC has better sensitivity out to a redshift of 0.5 than GLAST has to >10 GeV gamma rays. Similarly, at the longest timescales the ability of HAWC to detect emission at the highest energies (>100 GeV) is comparable to the sensitivity of GLAST above 10 GeV for Galactic objects. In the figure it is assumed that the source spectrum is $dN/dE \propto E^{-2}$ without a cutoff. (The only cutoff arising from the attenuation by the EBL.)

A more ambitious project would be to construct a similar but larger array (100,000 m^2) at an altitude of 5200 m. This detector is referred to as HAWC100 in the remainder of this paper. Based upon Figure 3 one can crudely calculate a trigger area of ~20,000 m^2 at 100 GeV for such an instrument. After accounting for reconstruction inefficiencies (including a background rejection criteria) one could expect an effective area of about 10,000 m^2 at 100 GeV for this type of instrument. The low-energy response would allow for the detection of gamma-ray bursts at larger redshifts than current instruments ($z \sim 1$ for HAWC100 compared to $z \sim 0.3$ for Milagro if, at the source, the TeV fluence is equal to the keV fluence). While current instruments, such as Milagro, indicate that the typical TeV fluence from a GRB is less than the keV fluence [74, 75], instruments such as HAWC100 and HAWC would be sensitive to a TeV fluence 2-3 orders of magnitude smaller than the keV fluence of the brightest gamma-ray bursts. A proposal to construct an instrument similar to this at the YangbaJing Cosmic-Ray Observatory in Tibet (elevation 4300 m above sea level) is currently under consideration [76].

The approach taken by the Tibet ASγ collaboration is to construct an array with excellent sensitivity at the highest energies. Their planned future instrument is referred to as Tibet MD (Tibet with Muon Detector). The Tibet MD collaboration is planning on installing over 9500 m^2 of muon detector within an expanded (to 83,000 m^2) ASγ array

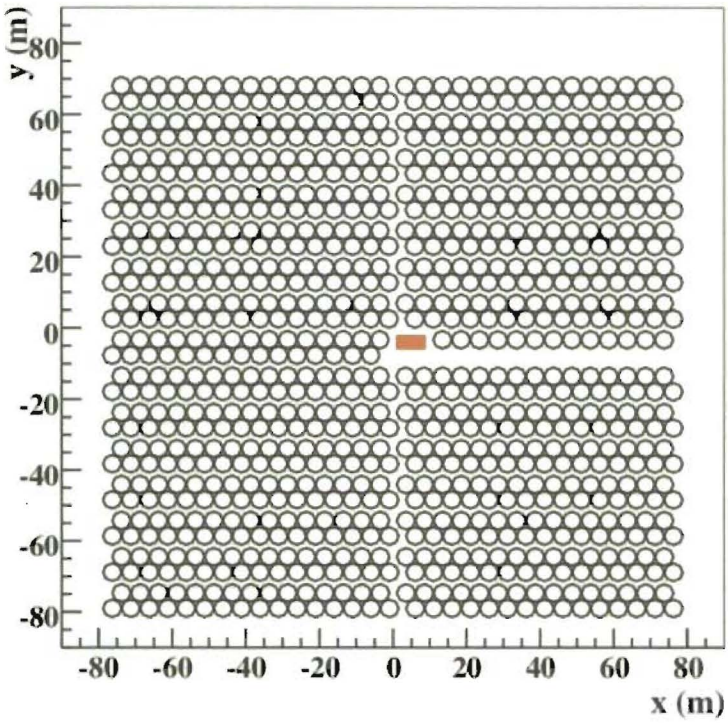

Figure 21. The HAWC detector. Each tank measures 4.3 m tall by 5 m diameter. The tanks are arranged in a close-packed grid with 5m spacing between tanks.

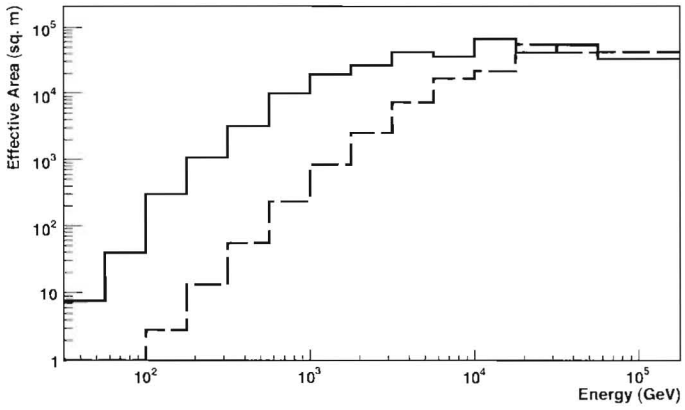

Figure 22. The effective area of the HAWC (blue/upper lines) and Milagro (red/lower lines) detectors. The solid lines show the area before background rejection cuts have been applied and the dashed lines after these cuts are applied. In both cases only events that are successfully reconstructed, within the analysis bin are counted.

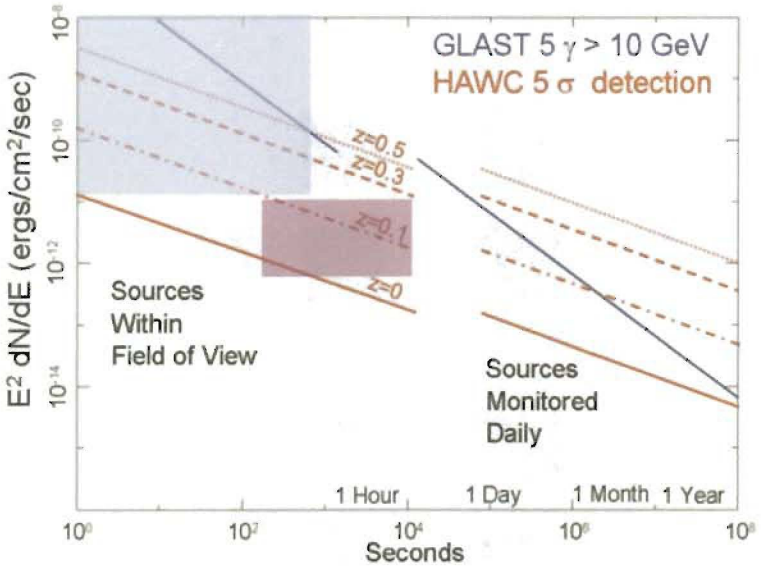

Figure 23. The sensitivity of GLAST and HAWC to transient phenomena as a function duration and energy flux. The blue line shows the GLAST sensitivity to >10 GeV gamma rays, where a detection threshold of 5 gamma-rays is required. For HAWC the sensitivity is shown for four different source redshifts (z=0,0.1,0.3, and 0.5). A 5 standard deviation detection is required in HAWC. The sources where assumed to have a differential spectral index of -2.0 and the model of Knieske et al. [71] was used to model the absorption due to the EBL. The blue shaded region delineates the parameter space typically occupied by gamma-ray bursts and the purple region the parameter space typically occupied by AGN flares. Figure courtesy of Brenda Dingus.

[78, 79]. Figure 24 shows the proposed layout of the detector. The muon detectors are water Cherenkov counters buried under 2.5 m of dirt. Each counter consists of a water pool measuring 7.2m×7.2m×1.5m deep, instrumented with two 20-inch Hamamatsu R3600 PMTs. The water pools are made from concrete and painted with a white epoxy resin. With this area of muon detector, the Tibet ASγ collaboration expects to be background free near $\sim$100 TeV (see Figure 9). In a background free environment the sensitivity is simply given by the number of detected gamma rays required to claim a signal, typically 10, divided by the array area and the time spent on source. This leads to a predicted sensitivity of $\sim 10^{-13}$ ergs cm^{-2}sec^{-1} at 100 TeV after a single year of observation. This is a factor of $\sim$100 better than the sensitivity of the CASA array [77] at 100 TeV.

Figure 25 shows the point-source sensitivity of current and future all-sky gamma-ray instruments. For comparison the sensitivity of GLAST and VERITAS/H.E.S.S. are shown. For the all-sky instruments the sensitivity is calculated for a 5-year exposure and averaged over the field-of-view of the instruments. The all-sky instruments can observe at least 2π sr of the sky with this level of sensitivity. (GLAST will survey the entire

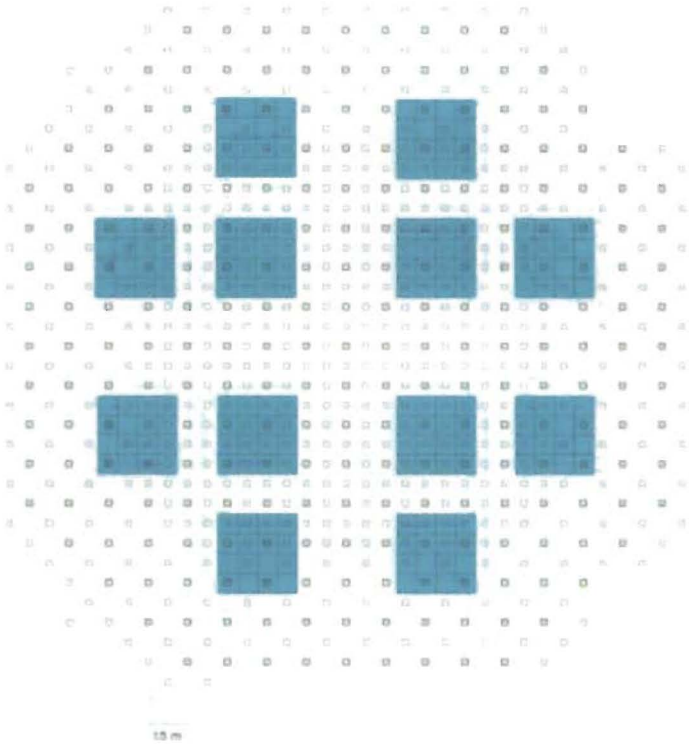

Figure 24. Schematic view of the Tibet MD array with the proposed muon detectors. The muon detectors are buried under 2.5m of dirt.

4π sr of the sky with the level of sensitivity indicated.) The sensitivity of the IACTs is given for a 50 hour exposure.

These future projects, in conjunction with the current and planned IACT arrays, will give us an unprecedented view of the high-energy universe. With it's low-energy response and high sensitivity above 10 TeV, HAWC will be able to observe flaring active galaxies, possibly detect the highest energy emission from gamma-ray bursts, and make a detailed map of the Galactic diffuse emission in TeV gamma rays. At the highest energies Tibet MD will study the end-point spectra of many Galactic objects. Their sensitivity is sufficient to detect most of the hard spectrum HESS sources above 100 TeV (if the power-law spectra of these sources continue to these energies), allowing for a more complete understanding of the limits to the particle acceleration processes that occur within our Galaxy and the origins of the cosmic radiation.

8. Conclusions

All-sky TeV gamma-ray observatories have made significant observations over the past decade. The previous generation of instruments lacked the sensitivity required detect even a single source of TeV gamma rays. The technological advances that made many

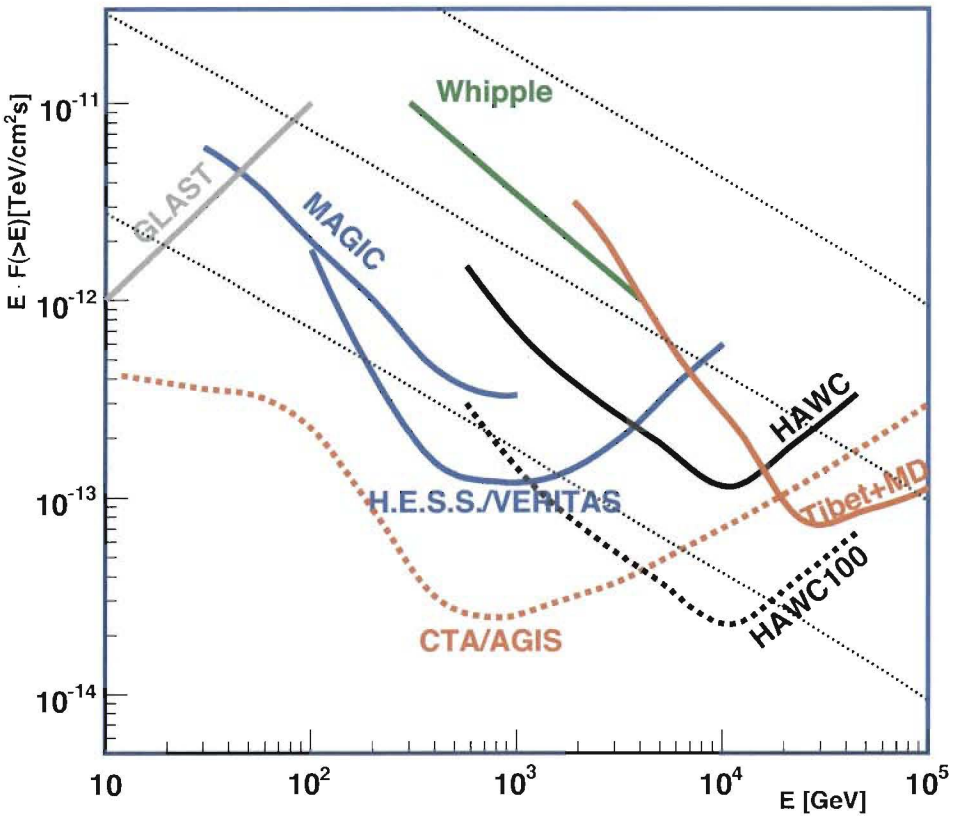

Figure 25. Point source sensitivity of current and future gamma-ray observatories to constant sources. For pointed instruments (H.E.S.S./VERITAS) the sensitivity is shown for a 50 hour exposure to a single source. For all-sky instruments such as GLAST, Tibet+MD, HAWC, and HAWC100 the sensitivity shown indicates the level at which these instruments will survey the sky that is visible to them (typically 2π sr, 4π for GLAST) after five years of operation.

of these detections possible were the application of water Cherenkov technology to the field and the construction of an array at extreme altitude.

The first detection of the Galactic diffuse emission above a TeV has indicated that the cosmic-ray spectrum may vary throughout the Galaxy and has given an indication of the location of possible cosmic-ray acceleration sites (the Cygnus Region). A class of extended sources has also been discovered, most of which are coincident with GeV sources detected by EGRET. It is likely that these are pulsar wind nebula. These sources

have hard spectra and the ability to accelerate particles to at least 20 TeV. Finally, both Tibet and Milagro have detected emission from extragalactic objects, demonstrating the capability of future all-sky instruments.

It is clear that the field of gamma-ray astronomy requires both IACTs and EAS arrays to gain a true understanding of the high-energy universe. The IACTs have unrivaled angular resolution (0.05-0.1 degrees) and therefore the capability to map extended Galactic sources. This capability coupled with x-ray, optical, and radio maps will lead to a much better understanding of the individual sources. The IACTs also have significantly better energy resolution than the all-sky instruments. In addition to enabling a better understanding of astrophysical sources, this could also allow them to identify the gamma rays resulting from the annihilation of dark matter. However, the all-sky instruments have the unique capability to continuously view a large region of the sky. This feature makes them well suited to study the transient high-energy universe. Despite over a decade of study since the first detection of an extragalactic object [20] we still do not know the duty cycle of TeV flaring activity in active galaxies and we have yet to detect >100 GeV emission from gamma-ray bursts. The next generation of all-sky instruments hold the promise of enabling such observations. Given the observed flaring nature of the known active galaxies it is expected that an instrument such as HAWC could detect many TeV flares in a single year. These new instruments will provide an unprecedented view of the Galactic diffuse emission that will lead to a better understanding of the distribution and spectrum of cosmic ray electrons and protons throughout our Galaxy. If this next generation of all-sky instruments is constructed we can look forward to another decade of discovery at the very-high-energy frontier.

9. Acknowledgements

This work is partially supported by the National Science Foundation, the Department of Energy Office of Science, and Los Alamos National Laboratory. I would like to thank Zhen Cao for his assistance with information regarding the ARGO detector and Hu Hongbo for his help in understanding the Tibet ASγ detector, Andrew Smith who performed the simulations for the HAWC detector and supplied Figures 5 and 10, Masato Takita for supplying Figure 9 and discussions on the Tibet+MD detector, and Brenda Dingus for supplying Figure 23. Finally, I would like to acknowledge the support of Los Alamos National Laboratory, which enabled not only the writing of this article, but also the construction and operation of Milagro.

References

[1] Alexandreas D E, *et al.* 1992 *Nucl. Instrum. Meth. A* **311**, 350
[2] Borione A, *et al.* 1994 *Nucl. Instrum. Meth. A* **346**, 329
[3] Atkins R W, *et al.* 2003 *Astrophys. J.* **595**, 803
[4] Amenomori M, *et al.* 2005 *Proc. 29th ICRC* Pune, India
[5] Martello D *for the ARGO collaboration*, 2007 to appear in *Proc. 30th ICRC*, Merida, Mexico

[6] Ong R, 1998 *Physics Reports* **305**, 93
[7] Hoffman C M, Sinnis C, Fleury P, Punch M, 1999 *Rev. Mod. Phys.* **71**, 897
[8] Amenomori M, *et al.* 2005 *Proc. 29th ICRC 2005* Pune, India
[9] Amenomori M, *et al.* 1999 *Astrophys. J.* **525**, L93
[10] Abdo A A, *et al.* 2007 *Astrophys. J.* **658**, L33
[11] Rossi B. and Greisen K. 1941 *Rev. Mod. Phys.* **13**, 240
[12] Crewther I Y and Protheroe R J 1990 *J. Phys. G: Nucl. Phys.* **16** L13
[13] Heck D, Knapp J, Capdevielle J N, Schatz G, and Thouw T, 1998 *Forschungszentrum Karlsruhe Report FZKA 6019*
[14] Bussino S and Mari S M 2001 *Astropart. Phys.* **15**, 65
[15] Atkins R W, *et al.* 2004 *Astrophys. J.* **608**, 680
[16] Amenomori M, *et al.*, 2005 *Proc. 29th ICRC*, Pune, India
[17] Wang Y, *et al.* 2008 *Preprint* arXiv:0804.1862v2
[18] Alexandreas D E, *et al.* 1993 *Nucl. Instrum. Meth. A* **328** 570
[19] Sinnis G, 2007 *Proc. 30th ICRC*, Merida, Mexico
[20] Punch M, *et al.*, 1992 *Nature* **358**, 477
[21] Stecker F W and Scully S T 2008 *Astron. and Astrophys.* **478**, L1
[22] Hartman R C, *et al.*, 1999 *Astrophys. J. Supp.* **123**, 79
[23] Lamb R C and Macomb D J, 1997 *Astrophys. J.* **488**, 872
[24] Abdo A A, *et al.*, 2007 *Astrophys. J. Lett.* **664**, L92
[25] Amenomori M, *et al.* 2007 *Proc. 30th ICRC*, Merida, Mexico
[26] van der Hucht K A, 2001 *New Astron. Rev.* **45**, 135
[27] Bochkarev N G and Sitnik T G, 1985 *Astrophys. Space. Sci.* **108**, 925
[28] Green D A, 2004 *Bull. Astron. Soc. India* **32**, 325
[29] Aharonian F, *et al.* 2005 *Astron. and Astrophys.* **431**, 197
[30] Mukherjee R, *et al.*, 2000 *Astrophys. J.* **542**, 740
[31] Djannati-Atai A, *for the HESS collaboration* 2007 *Preprint* arXiv:0710.2418v1, to appear in *Proc. 30th ICRC* Merida, Mexico
[32] Pavlov G G, Sanwal D, and Zavlin V E, 2006 *Astrophys. J.* **643**, 1146
[33] Aharonian F, *et al.*, 2007 *Astron. and Astrophys.* **472**, 489
[34] Aharonian F, *et al.*, 2006 *Astron. and Astrophys.* **406**, 265
[35] Hunter S D, *et al.* 1997 *Astrophys. J.* **481**, 205
[36] de Boer W, *et al.*, 2005 *Astron. and Astrophys.* **444**, 51
[37] Strong A W, Moskalenko I V, and Reimer O, 2004 *Astrophys. J.*, **613**, 962
[38] Strong A W, *et al.*, 2004 *Astron. and Astrophys.* **422**, L47
[39] Gralewicz P, *et al.*, 1997 *Astron. and Astrophys.* **318**, 925
[40] Huentemeyer P *for the Milagro collaboration*, 2007 to appear in *Proc. 30th ICRC*, Merida, Mexico, 0654
[41] Binns W R, *et al.*, 2005 *Astrophys. J.* **634**, 351
[42] Hall D L, Duldig M L, and Humble J E, 1996 *Space Science Reviews* **78**, 401
[43] Andreyev Yu M, Kozyarivsky V A, and Lidvansky A S, 2008 *Preprint* arXiv:0804.4381
[44] Amenomori M, *et al.*, 2006 *Science* **314**, 439
[45] Compton A H and Getting I E, 1935 *Phys. Rev.* **47**, 817
[46] Kolterman B E *for the Milagro collaboration*, 2007 to appear in *Proc. 30th ICRC*, Merida, Mexico
[47] Abdo A A, *et al.* 2008 *submitted to Astrophys. J.*
[48] Nagashima K, *et al.* 1989 *Nuovo Cimento C* **12**, 695
[49] Nagashima K, Fujimoto K and Jacklyn R M 1998 *J. Geophysical Research* **103**, 17429
[50] Ptuskin V S, Jones F C, Seo E S, and Sina R, 2006 *Advances in Space Research* **37**, 1909
[51] Strong A, Moskalenko I and Ptuskin V, 2007 *Ann. Rev. of Nucl. and Part. Sci.* **57**, 285
[52] Walker G *for the Milagro collaboration*, 2007 to appear in *Proc. 30th ICRC*, Merida, Mexico, 0672
[53] Han J L, *et al.* 2006 *Astrophys. J.* **642** 868

[54] Drury L and Aharonian F A, 2008 *preprint* arXiV:0802.4403v2
[55] Salvati M and Sacco B, 2008 *preprint* arXiV:0802.2181v1
[56] McEnery, J E, Moskalenko I V, and Ormes J F, 2004 *Preprint* arXiv:0406250v1
[57] Sadrozinski, H F-W, 2001 *Nucl. Instrum. Meth. A* **466**, 292
[58] Gehrels N and Michelson P, 1999 *Astropart. Phys.* **11**, 277
[59] Ferenc D, *et al.* 2005 *Nucl. Instrum. Meth. A* **553**, 274
[60] Fort J A i, *et al.* 2005 *Astropart. Phys.* **23**, 493
[61] Aharonian, F A, *et al.* 2006 *Astron. and Astrophys.* **457** 899
[62] Weekes T C, *et al.* 2002 *Astropart. Phys.* **17**, 221
[63] Abassi R U, *et al.* 2008 *Phys. Rev. Lett.* **100**, 101101
[64] The Pierre Auger Collaboration, Abraham J, *et al.* 2007 *Science* **318**, 938
[65] Aharonian F A, *et al* 2003 *Astrophys. J.* **636**, 777
[66] Akerlof C, *et al.* 1999 *Nature* **398**, 400
[67] Vestrand T W, *et al.* 2006 *Nature* **442**, 172
[68] Berger E, *et al* 2005 *Astrophys. J.* **629**, 328
[69] Keida D 2005 *Proceedings of Cherenkov 2005: Towards a Network of Atmospheric Cherenkov Detectors VII* p 437
[70] Gonzalez M M *for the HAWC collaboration* 2007 to appear in *Proc. 30th ICRC*, Merida, Mexico, 1250
[71] Kneiske T M, Bretz T, Mannheim K, and Hartmann D H 2004 *Astron. and Astrophys.* **413**, 807
[72] Veron-Cetty M-P and Veron P, 2006 *Astron. and Astrophys.* **455**, 773
[73] Aharonian F A, *et al* 2006 *Science* **314**, 1424
[74] Abdo AA, *et al.* 2007 *Astrophys. J.* **666**, 361
[75] Atkins R A, *et al.* 2005 *Astrophys. J.* **630**, 996
[76] Cao Z, 2008 *private communication*
[77] Borione A, *et al.* 1997 *Phys. Rev. D* **55**, 1714
[78] Takashi S *for the Tibet ASγ collaboration* 2007 to appear in *Proc. 30th ICRC*, Merida, Mexico, 0416
[79] Takashi S *for the Tibet ASγ collaboration* 2007 to appear in *Proc. 30th ICRC*, Merida, Mexico, 0417